Materials Science and Engineering C 75 (2017) 957–968

Contents lists available at ScienceDirect

Materials Science and Engineering C

journal homepage: www.elsevier.com/locate/msec

In vitro and *in vivo* characterization of anodised zirconium as a potential material for biomedical applications

Maria R Katunar [a,*], Andrea Gomez Sanchez [a], Ana Santos Coquillat [b], Ana Civantos [c], Enrique Martinez Campos [b], Josefina Ballarre [a], Tamara Vico [a], Matias Baca [d], Viviana Ramos [c], Silvia Cere [a]

[a] INTEMA, Universidad Nacional de Mar del Plata-CONICET, Juan B. Justo, 4302, B7608FDQ, Mar del Plata, Argentina
[b] Instituto de Estudios Biofuncionales, Universidad Complutense de Madrid, Madrid, España
[c] Instituto de Ciencia y Tecnología de Polímeros, CSIC, Madrid, Spain
[d] Traumatologia y Ortopedia, Hospital Interzonal General de Agudos "Oscar Alende", Mar del Plata, Argentina

ARTICLE INFO

Article history:
Received 30 September 2016
Received in revised form 14 December 2016
Accepted 24 February 2017
Available online 27 February 2017

Keywords:
Osseointegration
Zirconium implant
Anodisation
Animal model
Osteoclast
Osteoblast

ABSTRACT

In vitro studies offer the insights for the understanding of the mechanisms at the tissue–implant interface that will provide an effective functioning *in vivo*. The good biocompatibility of zirconium makes a good candidate for biomedical applications and the attractive *in vivo* performance is mainly due to the presence of a protective oxide layer. The aim of this study is to evaluate by *in vitro* and *in vivo* approach, the influence of surface modification achieved by anodisation at 30 and 60 V on zirconium implants on the first steps of the osseointegration process. In this study cell attachment, proliferation and morphology of mouse myoblast C2C12-GFP and in mouse osteoprogenitor MC3T3-E1 cells was evaluated. Also, together with the immune system response, osteoclast differentiation and morphology with RAW 264.7 murine cell line were analysed. It was found that anodisation treatment at 60 V enhanced cell spreading and the osteoblastic and osteoclastic cells morphology, showing a strong dependence on the surface characteristics. *In vivo* tests were performed in a rat femur osteotomy model. Dynamical and static histological and histomorphometric analyses were developed 15 and 30 days after surgery. Newly formed bone around Zr60V implants showed a continuous newly compact and homogeneous bone just 15 after surgery, as judged by the enhanced thickness and mineralization rate. The results indicate that anodising treatment at 60 V could be an effective improvement in the osseointegration of zirconium by stimulating adhesion, proliferation, morphology, new bone thickness and bone mineral apposition, making zirconium an emerging candidate material for biomedical applications.

1. Introduction

Metallic alloys are used in surgery due to their high mechanical and corrosion resistance in physiologic media [1]. The corrosion resistance in body fluids achieved by permanent prosthesis devices is due to the formation of a passive oxide that inhibits the transport and migration of metallic ions from the base metal to the nearby tissue [2]. It has been extensively proved that the success or failure of the osseointegration process is determined by the surface characteristics in different space length scales [3,4], and those materials where osseointegration occurs, have a lower implant replacement rate [4]. It is well known that the clinical success of orthopaedic implants depends on two main factors: initial fixation due to osseointegration in the first few months; and maintenance of the fixation over the long term [5]. Contact osteogenesis is responsible for colonization of an implant surface by osteogenic cells followed by the synthesis of extracellular bone matrix and subsequent appositional *de novo* bone formation [6] and is likely to be affected by the material used in implant fabrication.

Cementless prosthesis relies on the process of osseointegration for their incorporation into the bone and long-term survival. It has been suggested to have the minimal stress shielding and even superior survival rate [7–9] which make them the primary choice for young patients. Surface modification in cementless prosthesis can be considered as a tool to generate a surface that can provide a protective action together with a bioactive surface to integrate the metal to the human body [10,11]. A variety of surface modifications have been studied and applied to implants to achieve long-term fixation to the host bone by osseointegration. It is well known that rough surfaces promote cell commitment to the osteoblastic lineage and support higher expression of phenotype-specific markers [12–16]. However, although the cellular pathways involved in the biologic responses to implant surfaces are being progressively elucidated, and it has been recently shown that

* Corresponding author at: INTEMA, Applied Electrochemistry Division, UNMdP-CONICET, Juan B. Justo, 4302, B7608FDQ, Mar del Plata, Argentina.
E-mail address: mkatunar@fi.mdp.edu.ar (M.R. Katunar).

http://dx.doi.org/10.1016/j.msec.2017.02.139
0928-4931/

rough topography modulates the activation of Wnt/b catenin signalling in cells of the mesenchymal line, little is known about the characteristics of the ideal topography capable to maximize bone growth.

The osteoclasts, the bone resorbing cells, are crucial in bone regeneration process. Bone remodelling is the predominant metabolic process regulating bone structure and function during adult life, being the osteoclast the key participants [17]. The interaction between osteoblasts and osteoclasts or even the role of osteoclasts on the longevity of the implants is underestimated [18]. Osteoblasts were frequently considered to be the most dominating cells for osseointegration of implants since they are not only solely responsible for the generation of bone extracellular matrix but also for the regulation of osteoclasts differentiation and activity [19]. However, all the mechanisms related to the osteoclastic activity in the implant site are poorly understood. The difficulty in the isolation procedures *in vitro* and the low number of osteoclasts formation under physiological conditions, results in extremely limited investigations based on osteoclasts [18]. RAW 264.7 murine cell line has proven to be an important tool for *in vitro* studies of osteoclast formation and function [20]. This cell line belongs to cells of immune system which arrives in the first place to the damage tissue [21]. All the biomaterial implants have the capacity to induce a foreign body reaction (FBR); however the severity and clinical manifestation of these responses can widely differ [22]. This initial cell response can increase or reduce the osseointegration of the biomaterial [23,24].

Among the materials commonly used in prosthesis devices, zirconium (Zr) and its alloys are considered as potential candidates due to their low electronic conductivity, high corrosion resistance and biocompatibility [25]. They present greater strength, lower cytotoxicity and lower magnetic susceptibility than Titanium (Ti) [26]. It has been demonstrated that an artificial increase of the thickness and changes in the topography of the native oxide, will result in very strong reinforcement of the bone response [27,28]. Anodisation is an electrochemical process that grows an oxide by means of an anodic process. The oxide thickness formed by anodization varies from a few nanometers to a hundred of micrometres. It has been demonstrated that the chemistry and the topography of the surface oxide formed by Zr anodisation in phosphoric acid are simultaneously modified [29]. The oxide formed on the surface is mainly monoclinic ZrO_2 with the incorporation of phosphates from the electrolyte increasing the corrosion resistance of the anodised samples when compared with the untreated ones. The preliminary *in vivo* test demonstrated that sixty days after surgery osseointegration was observed for both anodized and non-anodized samples, and although there is an increase in bone mineral apposition for the anodized samples the quality, kinetics of growing and maturity are not well established [30–32]. Since the primary interaction between the tissue and the implant in through the surface, the understanding of their interaction for long term service deserves further research. The aim of this study was to evaluate by means of an *in vitro* and an *in vivo* approach, the influence of surface modification achieved by anodisation at 30 and 60 V on zirconium implants on the first steps of the osseointegration process.

2. Materials and methods

2.1. Implants and surface treatment

Commercially pure zirconium cylinders (99.5% Roberto Cordes S.A., Argentina) of 40–50 mm length and 1 mm diameter were used for the *in vivo* tests and plane samples of 1 cm^2 for the *in vitro* assays. Three surface conditions were compared: *as received* pure zirconium (Zr0, control), zirconium anodised at a constant potential of 30 V (Zr30) and at 60 V (Zr60) during 60 min in 1 mol $L^{-1} \cdot H_3PO_4$. All samples were mechanically polished with 600 grit emery paper, degreased with ethanol and rinsed with deionized water. The sample conditioning and oxide growth details have been previously reported [33].

2.2. In vitro studies

2.2.1. Cell culturing

Zirconium plates of 1 cm^2 were autoclaved and washed with completed medium previous to cell seeding. Three procedures of seeding were performed.

a) Seeding with C2C12-GFP. This is a mouse pre-myoblast cell line (ATCC® CRL 1772™). Green Fluorescent Protein (GFP) was expressed due to previous lentivirus infection of this cell line allowing to be evaluated through an opaque material. Routine passaging of the cell line was performed with Dulbecco's Modified Eagle Medium (DMEM) (D6429, Sigma-Aldrich, St. Louis, MO), supplemented with 10% foetal bovine serum (FBS, Hyclone®, Thermo Scientific) plus antibiotics (100 U/mL penicillin and 100 μg/mL streptomycin sulphate; Sigma-Aldrich, St. Louis, MO). Cells were incubated at 37 °C with 5% CO_2 and the medium was refreshed every 2 or 3 days. C2C12-GFP cells were seeded on the materials with a density of 1×10^4 cells per cm^2. This cell line was evaluated by fluorescence microscopy (FITC filter λex/λem = 490/525 nm) at 24, 48, 72 and 96 h (h) to determine cell adhesion and growing on the material.
b) Seeding with MC3T3-E1 cell line (ATCC® CRL-2593™). This is a mouse preosteoblastic cell line. Cells were maintained in complete Alpha Modified Eagle medium (α-MEM A10490, Gibco, UK) without ascorbic acid supplemented with 10% foetal bovine serum (FBS, Hyclone®, Thermo Scientific) plus antibiotics (100 U/mL penicillin and 100 μg/mL streptomycin sulphate, Sigma-Aldrich, St. Louis, MO) incubated at 37 °C with 5% CO_2. For cell differentiation, cells were plated at 1×10^4 cells per cm^2 in completed maintenance medium with 50 μg/mL of ascorbic acid, 10 nM dexamethasone and 10 mM β-glycerol phosphate, complete differentiation medium was changed every 3 or 4 days
c) Seeding with RAW 264.7 cell line (ATCC® TIB-71™). This cell line was used as an osteoclast differentiation model from a mouse macrophage population. RAW cells were maintained in an undifferentiated state by culture in completed D-MEM (D6429, Sigma-Aldrich, St. Louis, MO) and the medium was changed every 3 days. For differentiation, cells were plated at 2×10^4 per cm^2 in completed medium (α-MEM, A10490, Gibco, UK) supplemented with 50 ng/ml of recombinant RANKL (PeproTech Inc. Rocky Hill, NJ) during 5 days, incubated at 37 °C with 5% CO_2.

2.2.2. Cell metabolic activity

Metabolic activity of MC3T3 was measured by Alamar Blue assay following the manufacturer's instructions (BioSource, Camarillo, CA). Assays were carried out bytriplicate on each sample type. This method is nontoxic, scalable and uses the natural reducing power of living cells, generating a quantitative measure of cell viability and cytotoxicity. Briefly, Alamar Blue dye (10% of the culture volume) was added to each sample with fresh medium, containing living cells seeded over the plates, and incubated for 90 min. The fluorescence (λex/λem 535/590 nm) of each well was measured at 72 and 168 h using a plate-reader (Synergy HT, BioTek).

2.2.3. Actin and Hoechst

Cells were fixed with 4% paraformaldehyde (PFA) solution for 15 min. After PFA was removed, cells were rinsed with PBS twice and permeabilized with 0.1% (v/v) Triton X-100, washed with PBS and stained with Texas Red®-X phalloidin (Life Technologies), a high-affinity F-actin probe conjugated to red fluorochrome, for 20 min at room temperature and in darkness, followed by Hoechst staining (Invitrogen, Molecular Probes ®) for nuclei visualization. Finally fluorescent-labelled cells were observed using an inverted fluorescence microscope (Olympus IX51) with a TRICT filter (λex/λem = 550/600 nm) for Actin and DAPI filter for

Hoechst (λex/λem = 380/455 nm) using CellD analysis software (Olympus).

2.2.4. TRAP (tartrate resistant acid phosphatase)

TRAP was studied using immunocytochemistry in order to evaluate RANKL-induced osteoclast differentiation over the samples. For TRAP staining rabbit anti-TRAP (1/200; Santa Cruz Biotechnology) and anti-rabbit (1/200; Millipore) antibodies were used. The staining protocol was performed as standard procedures (PFA 4% fixation; Blocking Solution: 5% Normal Donkey Serum; 0.3% Triton X-100 in 1× PBS). The visualization of the fluorescent-labelled cells was performed in an inverted fluorescence microscope (Olympus IX51) with a TRICT filter (λex/λem = 547/572 nm) using Cell D analysis software (Olympus).

2.3. In vivo studies

2.3.1. Animals

Twelve week-old male WKAH/Hok rats (n = 36) weighing 300–330 g were used in this study. The animals were divided in three groups for each type of surface treatment: control and anodised. All animals were housed in a temperature controlled room with a 12 h. alternating light–dark cycle and were given water and food *ad libitum* throughout the study. All the experiments were approved by the Bioethics Committee HIEMI-HIGA (Mar del Plata, October 2011).

2.3.2. Surgical procedure

Rats were anaesthetized with Ketamine/Xylazine (10 mg/kg; 10 mg/kg) according to their weight. The surgery region was cleaned with antiseptic. The animals were placed in a supine position and the implantation site was exposed through the superior part of the femur's internal face. A region of around 0.5 cm diameter was scraped in the femur plateau and a hole was drilled using a hand drill at low speed with a 0.15 cm diameter bur. The implants were placed bilaterally ensuing two implants per rat. The control and anodised implants were placed by press-fit into femur extending into the medullar canal. The wound was closed with conventional suture. X-ray radiographs were taken after surgery for control purposes.

2.3.3. Bone labelling with fluorochromes

A polychrome sequential fluorescent labelling method was used to characterize the new bone formation and mineralization. At 1, 2 and 4 weeks after surgery, different fluorochrome were administered intraperitoneally at a sequence of 30 mg/kg alizarin complexone (Sigma-Aldrich, USA), 20 mg/kg calcein (Sigma-Aldrich, USA).They bind to calcium ions and later can be incorporated at mineralization sites in the hydroxyapatite crystals. The animals were sacrificed 15 and 30 days after implantation. The fluorescent dyes can be detected in histological sections with a fluorescent microscope (Nikon Eclipse Ti, Tokyo, Japan) with appropriate filters giving an indication of new matrix deposition over time [33].

2.3.4. Histological analysis

Fifteen and thirty days after implantation, six rats with control and anodised implants, Zr30and Zr60V (all individuals from different litters) were deeply anaesthetised with Ketamine/Xylasine (100 mg/kg, 10 mg/kg) and sacrificed with an overdose of pentobarbital. The retrieved samples were cleaned from surrounding soft tissues and fixed in neutral 10 wt% formaldehyde for 24 h. Then they were dehydrated in a series of alcohol–water mixtures followed by a methacrylated solution and finally embedded in a polymethyl methacrylate (PMMA) solution and polymerized. The PMMA embedded blocks were cut with a low speed diamond blade saw (Buehler GmbH) cooled with water. Sections were made 100 μm thick and polished to a final thickness of about 60 μm for histological observations.

2.3.5. Histological observations

Proximal femur cross-sections transversal to the central long axis of the femur (n = 3p/surface treatment group) were prepared and cut as described above. Three sections from the proximal region were selected. Toluidine stain allows observation and identification/discrimination of tissues (*e.g.* bone and bone marrow) around the metal-implant interface without removing the PMMA before the histological examination in a light microscope (Nikon Eclipse Ti, Tokyo, Japan).

Histomorphometric analysis of the thickness of newly formed bone in contact with the implant was evaluated using the software ImageJ 1 (open source: http://rsb.info.nih.gov/ij/features.html). The area of the primary press-fit contact of the implant and bone was excluded from the analysis. Thus, only new bone was analysed in the study [34].

2.3.6. Mineral apposition rate (MAR)

The mineral apposition rate (MAR, μm/day) is the rate at which mineral accretion occurs at a remodelling site during the period of bone formation. MAR is a fundamental histomorphometric variable, and it is a reliable measure of osteoblast function. Fluorochrome sequential labelling was performed postoperatively to assess the time course of bone formation and mineralization as reported previously as describe above [35,36]. At 1, 2 and 4 weeks after surgery, different fluorochromes were administered intraperitoneally at a sequence of 30 mg/kg alizarin complexone (Sigma-Aldrich, USA), 20 mg/kg calcein (Sigma-Aldrich, USA). The nomenclature and symbols used in conventional bone histomorphometry are those describe by Parfitt et al. [37].

2.4. Statistical analysis

In this study, the data are shown in the form of mean value ± σ_{MEAN} (standard deviation of the mean). Differences between the groups were assessed by one way ANOVA and Tukey test were performed using GraphPad In Stat version 3.00 (Graph Pad Software). All statistical analysis was considered significant when p value < 0.05.

3. Results

3.1. Surface characteristics of zirconium

Fig. 1a presents the surface of as received zirconium (Zr0, control). Zirconium is covered in air with a thin native oxide film of thickness < 10 nm of Zr suboxides (paper David) that cannot be resolved in SEM images.

In Fig. 1b, c shows the SEM image corresponding to Zr30V and Zr60V respectively. Anodic films are characterized by the appearance of bright spots of sub micrometrical oxide structures, more evident in Zr60V than in Zr30V. There is also an increase in film thickness with potential in the nanometrical range (not resolved by SEM microscopy).The oxide structures are similar to those observed in titanium anodic films [38]. The incorporation of phosphate ions into anodic films growth in phosphoric acid was evidenced in a previous work [39]. Phosphate incorporation constitutes a major change in surface chemistry of anodized zirconium compared to as received condition.

3.2. Biocompatibility studies: cell adhesion and growth over Zr samples

3.2.1. In vitro response of premyoblastic C2C12-GFP cell line

In vitro biocompatibility of the materials was assessed in a preliminary study with the self- fluorescent premyoblastic cell line C2C12-GFP. This cell line can differentiate into myoblasts or, under a concrete stimuli (e.g. BMP-2) or environment, can transdifferentiate into osteoblasts. As it is described in Fig. 2, microphotographs were taken at 24, 48, 72 and 96 h to determine cell growth and adhesion to the material. At 24 h, cells growing over the three samples have an expanded morphology showing a suitable initial adhesion behaviour. Furthermore, in Zr30V and Zr60V (B and C) it can be appreciated a cell alignment

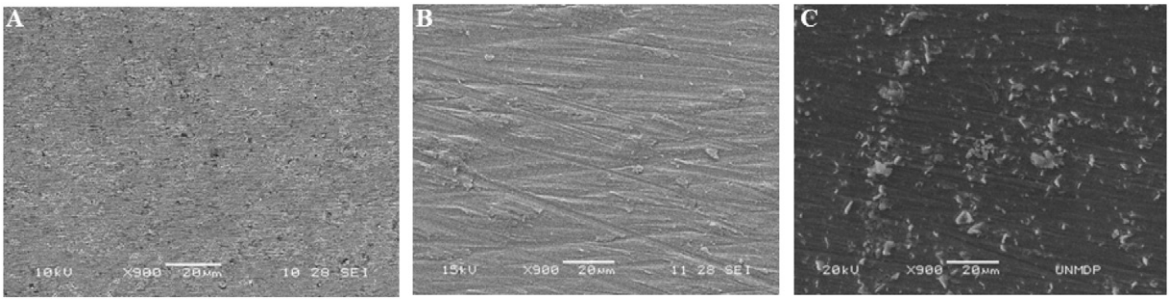

Fig. 1. Photomicrographs of zirconium samples with different surface treatments. (A) control, Zr0V (B) Zr30V and (C) Zr60V.

coinciding with the anodised treatment pattern that it is maintained until the end point (96 h). Regarding cell growth, cells proliferated along the days with a resulting formation of a cell sheet monolayer on all the samples.

3.2.2. In vitro response of osteoblastic MC3T3 cell line

Osteoblastic MC3T3 cell line possesses the critical properties in osseointegration rendering them suitable for the evaluation of osteogenic properties of bone substitutes. The initial adhesion behaviour and spreading of MC3T3 are monitored at different time points. After culturing for 72 h, MC3T3 culture were attached and spread onto the surface as shown in Fig. 3. The quantification of metabolic activity at 72 h and 168 h after seeding can be seen in Fig. 4.

The Alamar Blue *in vitro* results showed that all conditions under study were biocompatible and they did not inhibit cell proliferation Although there is no remarkable statistical difference between the anodised conditions, a sight tendency for enhanced metabolic activity can be detected on the Zr60V.

As it was detected with C2C12-GFP cell line, osteoblastic cells were also aligned following anodised treatments (Fig. 5).

3.2.3. Immune system: macrophage cell behaviour

RAW 264.7 macrophage cell line is a well recognized model in regenerative medicine to study immune system activation. With proper stimuli, this cell line can polarize into macrophagic M1 and M2 phenotypes, or fuse to form osteoclasts, bone resorbing cells. Cells were seeded over the materials without RANKL (osteoclastic signaling molecule) and as it was expected no osteoclast formation occurred. Cells grew homogeneously in all samples (Fig. 6).

In Zr60V macrophages are organized in lines with elongated morphology as the oxide treatment is displaced (Fig. 6G). This phenotype corresponds to a M2 polarized state, an optimal immune response for successful implant integration.

3.2.4. Osteoclast differentiation

Osteoclast formation induced by RANKL was achieved in all the samples (Fig. 7) as it can be seen in actin images (first row in red). Moreover, Hoechst staining (second row in blue) showed that the formed osteoclasts were mature as they have several nuclei. There were a major number of osteoclasts per area in Zr30V and Zr60V evidencing an increased differentiation capacity over Zr treatments. Cell alignment is also present in the osteoclast cytoskeleton (Fig. 7G) at Zr60V, consistent with the oxide treatment.

In order to elucidate the difference between Zr0 (Fig. 8A) and the treated samples in osteoclast differentiation, an immunocytochemistry of TRAP was performed. On Zr60V, more osteoclasts (Fig. 8B) were detected with increased resorption ability as many lysosomal vesicles are present (Fig. 8C).

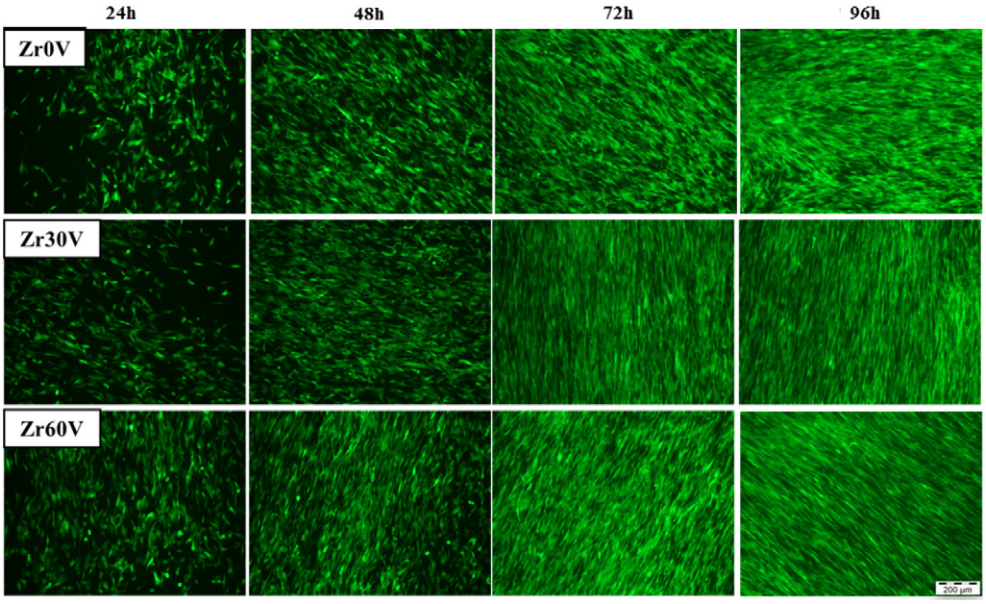

Fig. 2. C2C12-GFP cells seeded on Zr0V, Zr30V and Zr60V. Photos were taken at 24, 48, 72 and 96 h (end point). Cell alignment and tissue formation can be appreciated after 24 h.

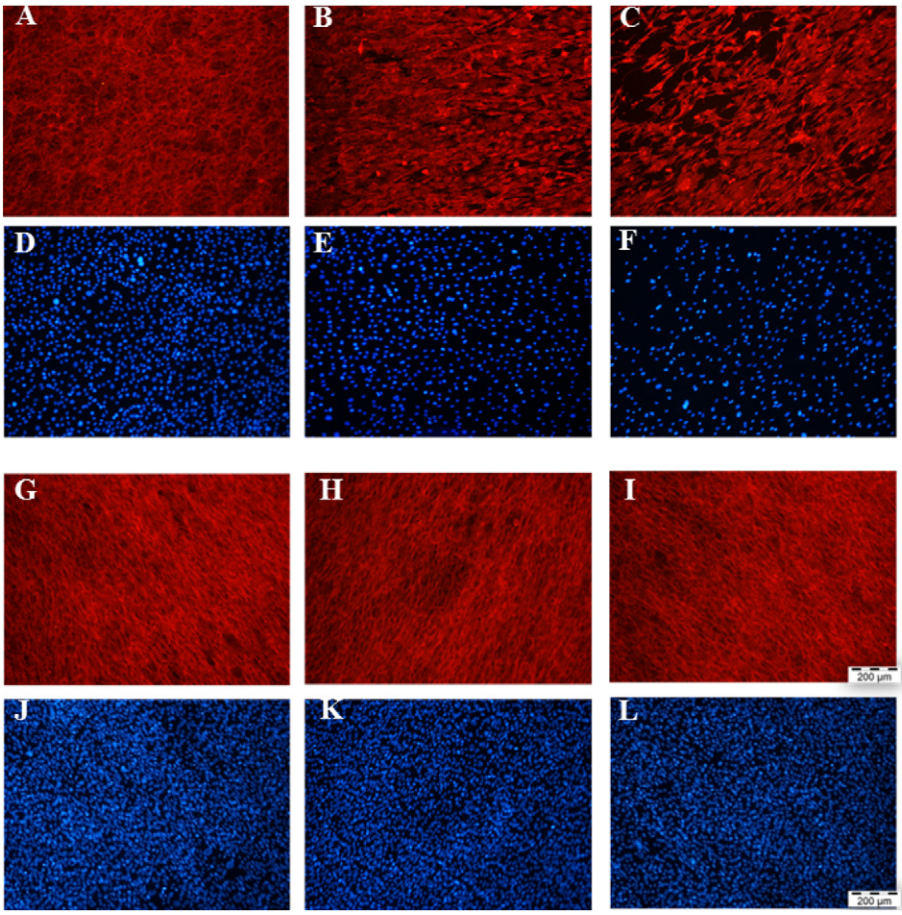

Fig. 3. MC3T3 proliferation over zirconium surfaces:72 h after seeding: A and D: Zr0V, B and E: Zr30V and C and F: Zr60V; 120 h after seeding: G and J:Zr0V, H and K: Zr30V and I and L: Zr60V. First and third row: actin staining (cytoskeleton). Second and fourth row: Hoechst staining (cell nuclei).

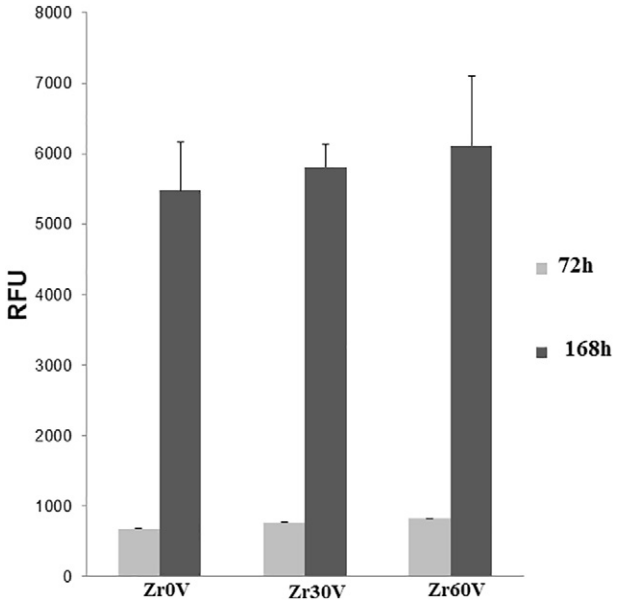

Fig. 4. Metabolic activity (Alamar Blue) of MC3T3 cell culture at 72 h and 168 h after cell seeding. RFU (Relative Fluorescence Units).

3.3. In vivo osteointegration of implant surface

3.3.1. Clinical observations

The animals recovered perfectly well after the surgery and neither signs of infection nor inflammation were noted upon clinical examination during the experiment.

3.3.2. Histological analysis and histomorphometry

Fig. 9 shows optical microscopy images of Toluidine blue stained section of the anodised implant sample after 15 and 30 days of implantation in a rat femur model. It is possible to distinguish the newly formed bone or *the novo* bone formation zone (with the implant in contact with the marrow medium). Histological analysis demonstrates that the characteristics of bone tissue integration around control and anodised implants are similar. Lamellar bone is continuous and in close contact in both metal surface implants (bone-implant contact). There is no fibrous tissue between the implant and the bone. Neither mononuclear cell accumulations (lymphocytes, monocytes), nor osteoclast are seen close to the implant.

Histomorphometric analysis revealed that 15 days after implantation there is a significant reduction in new bone thickness around Zr30V compared to control implants. Nevertheless, Zr60V shows a significant increase in new bone facing the implant compared to control and Zr30V. At 30 days after implantation no significant difference between the newly bone thickness facing the implant between control and anodised samples can be seen. It is interesting to highlight that control and Zr30V show a significant increase in new bone formation between 15 and 30 days after surgery while Zr60V implants show the

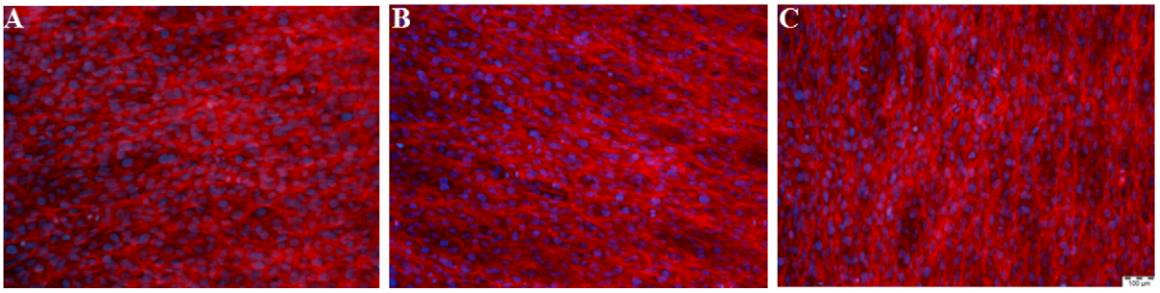

Fig. 5. MC3T3 proliferation over zirconium surfaces. A: Zr0V, B: Zr30V and C: Zr60V) at 120 h after cell seeding. Merge, red: actin staining (cytoskeleton); blue: Hoechst staining (cell nuclei). (For interpretation of the references to color in this figure legend, the reader is referred to the web version of this article.)

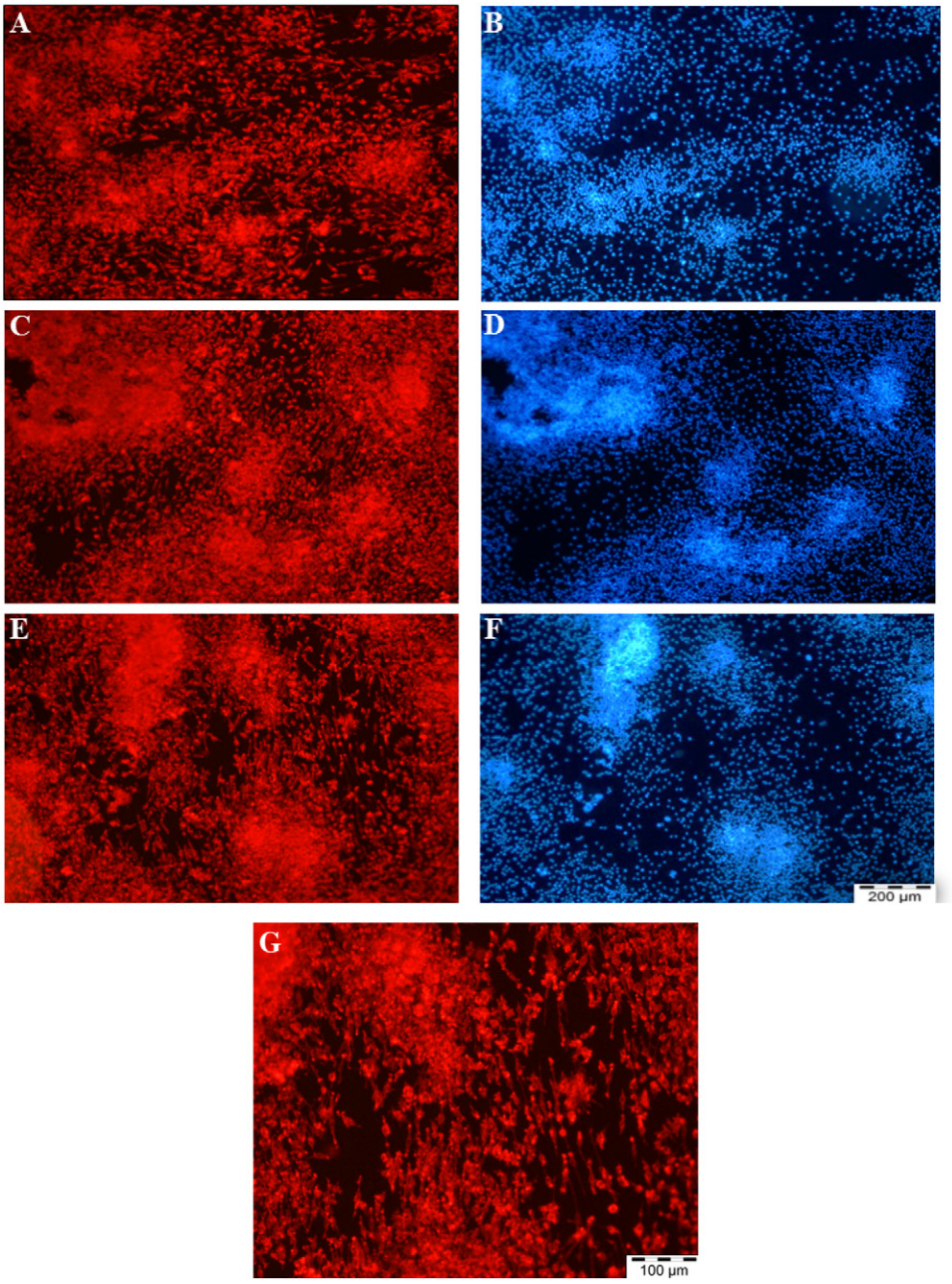

Fig. 6. Photomicrographs of actin (red) and Hoescht (blue) of RAW 264.7 cells growing homogenously between samples A and B: Zr0V, C and D: Zr30V and E and F: Zr60V.G: Detail of macrophages over Zr60V surface. Macrophages are organized in lines with elongated morphology as the oxide treatment is displaced. (For interpretation of the references to color in this figure legend, the reader is referred to the web version of this article.)

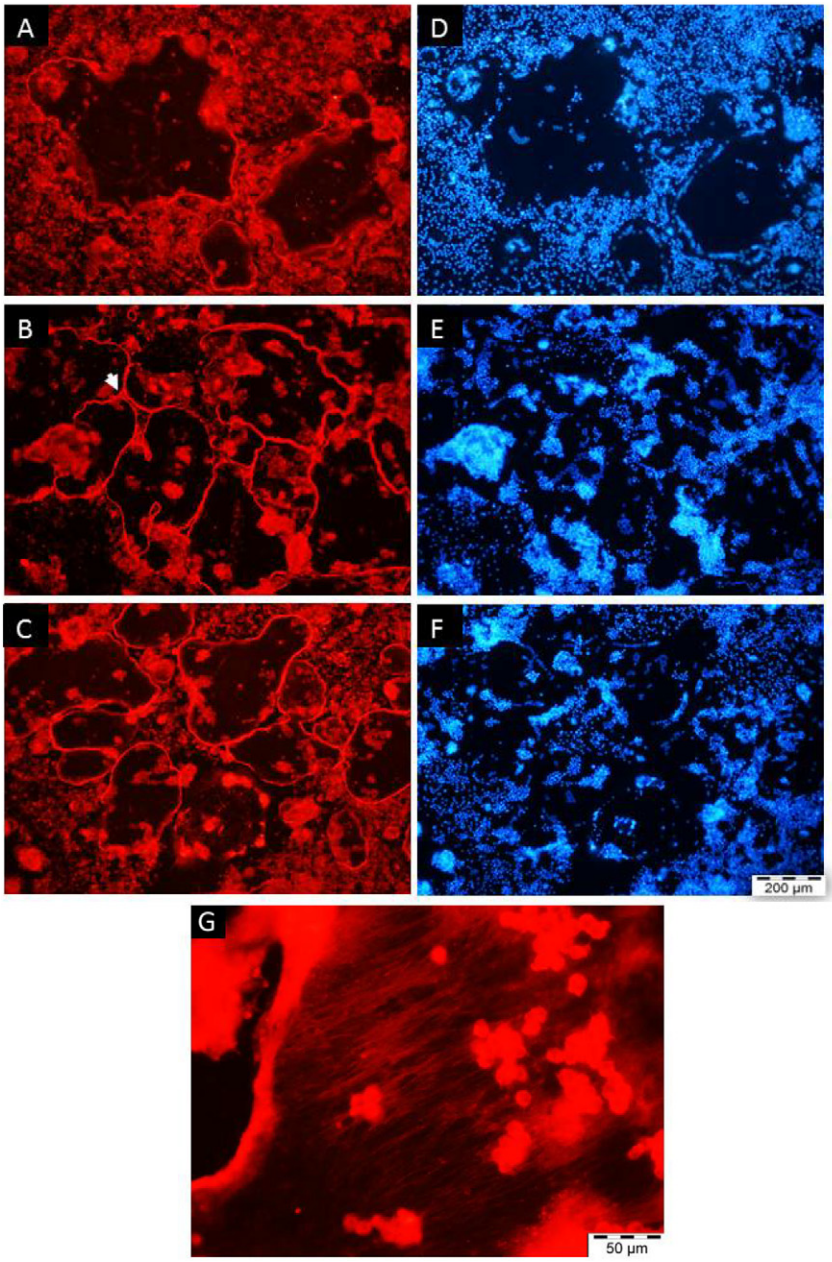

Fig. 7. Photomicrographs of actin (red) and Hoescht (blue) of RAW 264.7 cells forming multinucleated osteoclasts over zirconium surfaces. A and D: Zr0V, B and E: Zr30V and C and F: Zr60V. G: Detail of actin staining (400×) of an osteoclast growing on Zr60V·Filaments seems to follow the same orientation than the oxide treatment. (For interpretation of the references to color in this figure, the reader is referred to the web version of this article.)

highest new bone thickness in the firsts 15 days after implantation, being this thickness comparable to the one reached 30 days after surgery (Fig. 10).

3.3.3. Sequential fluorescent labelling analysis

Sequential fluorescent labelling (for 15 days and 30 days after implantation) is used to record and monitor new bone formation around the three implant groups by applying two types of fluorochromes. Fluorescent markers calcein and alizarin complexone were detected in control and anodised implants with the same distribution independently of the anodised condition. Fig. 11 shows calcein and alizarin complexone deposition around the implants 15 days after surgery. They are found to be deposited all around the implants showing an irregular and intense distribution both in control and anodised surfaces fifteen days after surgery. Nonetheless, Fig. 12 shows the sequential fluorescent labelling 30 days after surgery where fluorochrome distribution shows a more organized and clean profile both in control and anodised surfaces.

Fig. 13 shows mineral apposition rate (MAR) quantitative analysed 15 and 30 days after surgery in the bone ingrowth around the metallic implant in anodised at 30 V and 60 V when compared with controls. The results show a significant reduction in MAR parameter around Zr30Vand a significant increased around Zr60V implants both are compared with control. On the other hand, 30 days after surgery MAR parameters reach comparable values in control and anodised surfaces.

4. Discussion

Surface plays a key role in biomaterials performance since a different biological response can occur according to the surface properties of metallic biomaterials. Biomaterials can trigger a biological reaction from

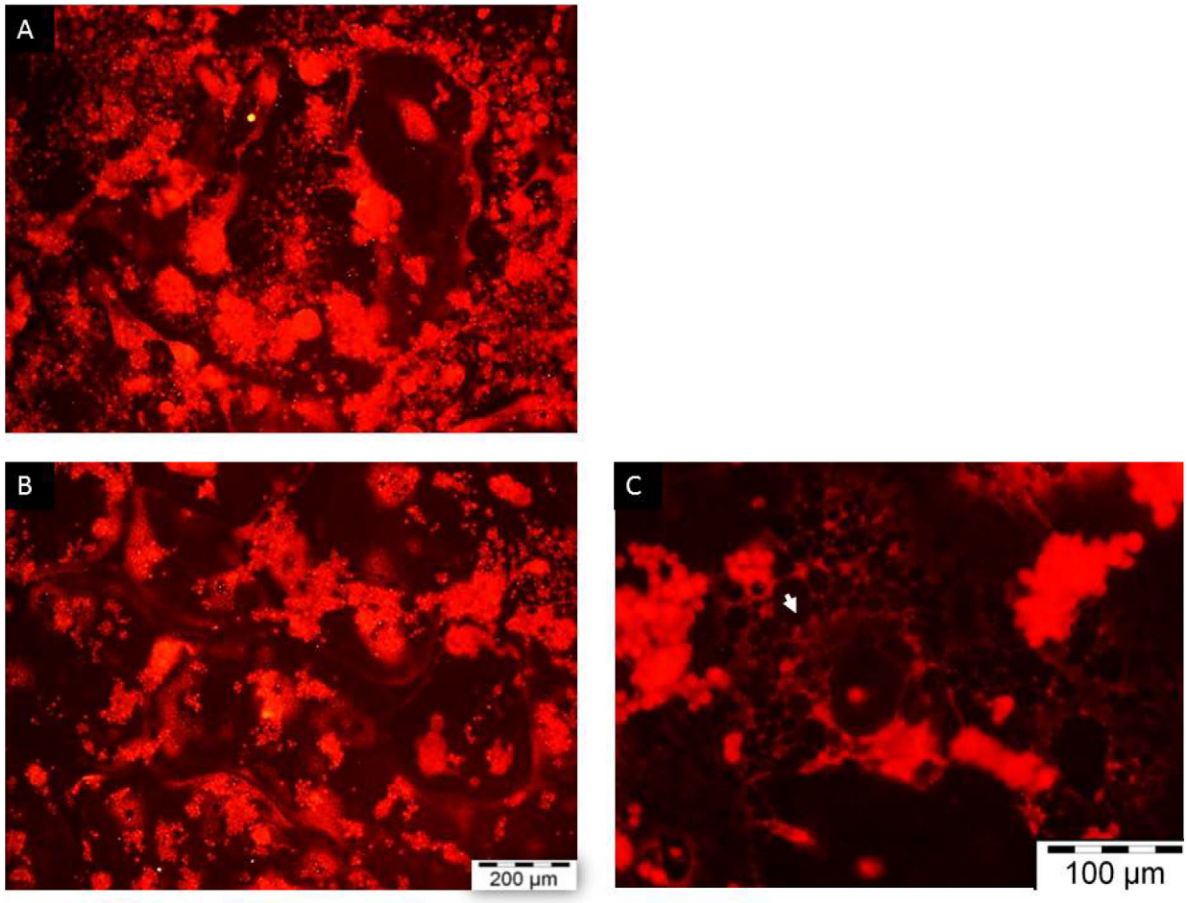

Fig. 8. Immunocytochemistry of Tartrate resistant acid phosphatase. RAW 264.7 cells forming multinucleated osteoclasts over the Zr0V (A) and Zr60V (B). C) Detail (200×) of Zr60V where osteoclasts are differentiated. Resorption phenotype is present as there are many lysosomal vesicles (see arrow).

the host after being implanted. An inappropriate metallic biomaterial surface can lead to an encapsulation of the material with dense connective tissue and a consequent isolation from the body fluid ending to a failure of the biomaterial [40]. On the other hand, the well-designed implant surface could form an interlock with the surrounding bone and achieve osseointegration, which indicates the biocompatibility of the

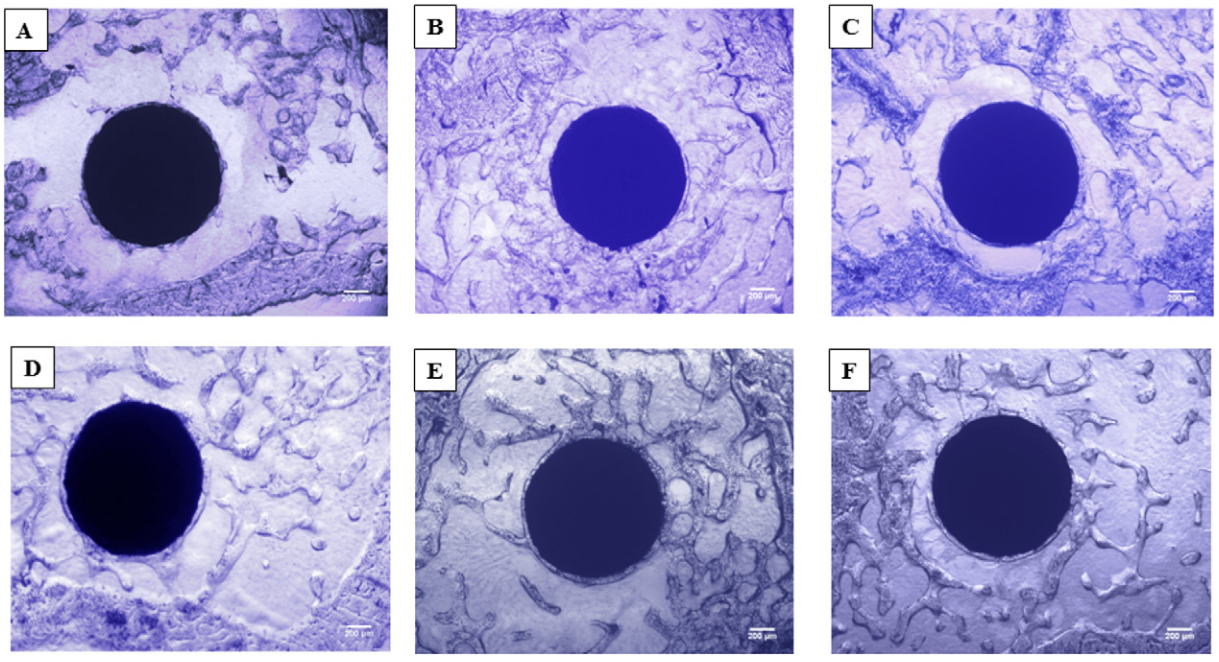

Fig. 9. Histology showing bone-implant interface in rat tibia cross-section 15 and 30 days after the implantation. A: Zr0V, B: Zr30V and C: Zr60V new bone formation 15 days after surgery. D: Zr0V, E: Zr30V and F: Zr60V new bone formation 30 days after surgery (staining: Toluidine blue, original magnification 40×).

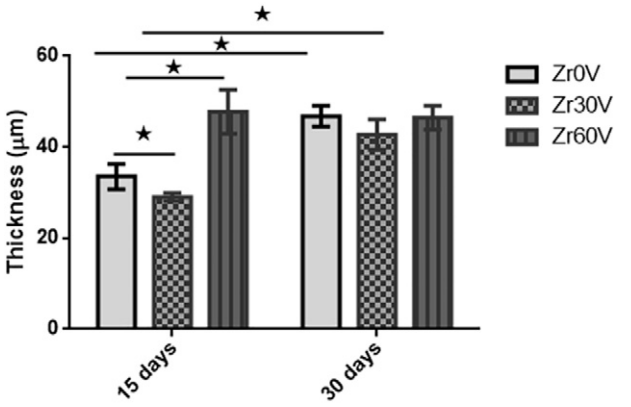

Fig. 10. Thickness of new bone layer on the implant surface in control and anodised implants 15 and 30 days after surgery. Data are expressed as mean ± SEM, $n = 6$ femur/group (by one way ANOVA and Tukey test).

metallic biomaterial. It has been demonstrated that changes in topography and chemistry of the surface greatly affect the tissue response in *in vivo* assays [27].Orthopaedic and dental implant fixation depends on both bone and bone-implant contact, and bone formation around implant. It is known that gaps at the interface between the implant and the bone increase the risk of failure in implant fixation, which may result in the loss of the piece [41].

The modification of implant surfaces is being investigated to improve the biocompatibility of biomaterials. The ability to "mimick" the biology of surrounding tissue or promote wound repair is thought to improve the integration of biomaterials and reduce the foreign body reaction [42–44]. It is known that methods of altering topography and chemistry are wide and varied [45–47]. These techniques result in differential surface geometries in the micro and nanometre scale, producing "rough" surfaces and in general, "rougher" surfaces have shown altered cell adhesion [48,49], density and spreading [50,51], modulated cytokines secretion [52,53], motility [54], enhanced proliferation and differentiation [50,55], and macrophage fusion [56]; however these responses are cell-specific and dependent on the method of surface modification. Additionally, surface roughness is further differentiated based on modified dimensions such as topography height, width, rigidity and spacing and patterns Pre-myoblastic and osteoblastic cells can recognize the implants surface able to attach and proliferate fast over Zr samples, forming a cell monolayer with suitable metabolic activity measures. Furthermore the surface treatment of the Zr samples induces cells growth into a define direction, and cluster cells are interconnected by a large number of filopodia, especially over Zr60V on which the cells nearly cover the whole surface, indicating that surface treatment alters not only the initial cellular adhesion of MC3T3 cells but also their morphology. These results are in agreement with some reports showing an enhance in osteoblast like cell attachment after 24 h on rough titanium, evidencing that surface topography also caused the alignment of cells parallel to the 10um grooves presented on the metal surface [57]. Due to implant surface properties (e.g. raw material, roughness or even porosity) macrophages will activate expressing a wide spectrum of polarization states which are characterized by the cytokine release profile of those cells. The pro-inflammatory phenotype "M1" of these cells induce fibrotic capsule and at the end failure of the biomaterial. However, the anti-inflammatory "M2" response controls the immune response, enhance blood vessel formation and wound healing [58,59]. Macrophage activation to M2 phenotype can be modulated by changing surface properties increasing the healing process and favouring long term implant stability. The results also show that initial immune system evaluation of Zr samples with macrophage precursors showed no polarization to M1 states, a precursor of foreign body giant cell apparition, fibrous tissue formation and implantation failure. In contrast, M2 elongated states were detected in Zr60V, a phenotype that will

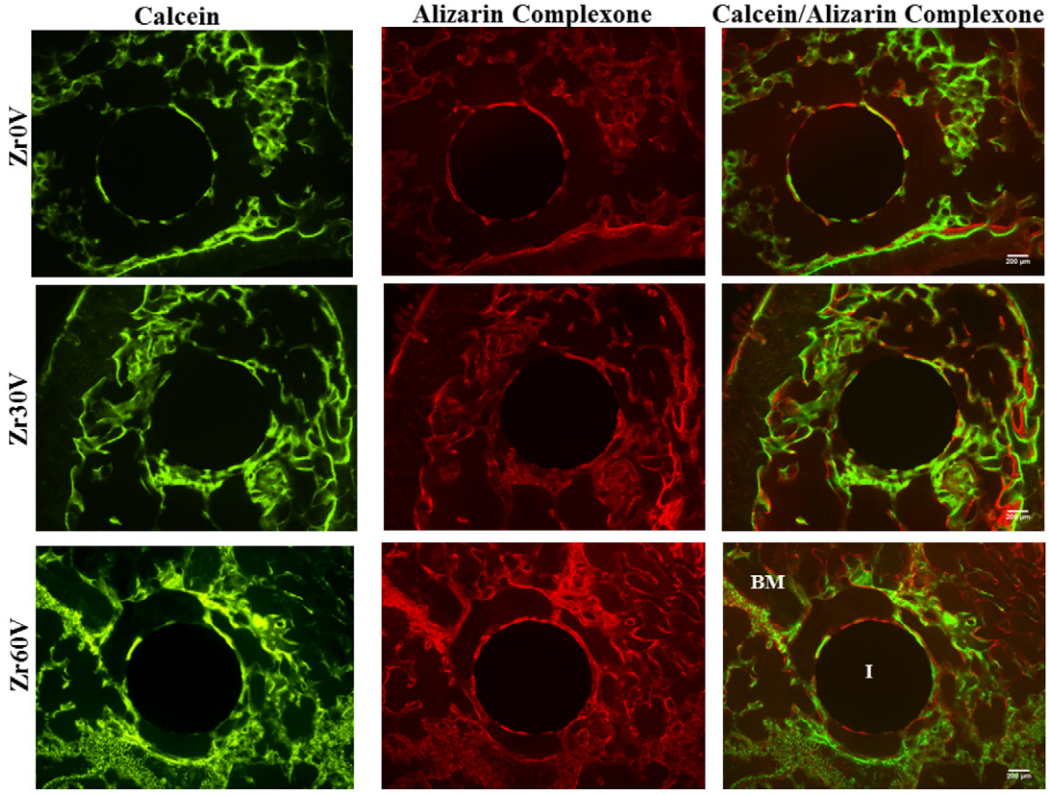

Fig. 11. Fluorescent microscopy image of rat tibia cross-sections with control and anodised implants 15 days after surgery. Green (Calcein) and red (Alizarin Complexone) lines are seen in the new bone around the implant (Imp) at 15 days after implantation, respectively. BM: bone marrow, I: implant (original magnification: 40×). (For interpretation of the references to color in this figure, the reader is referred to the web version of this article.)

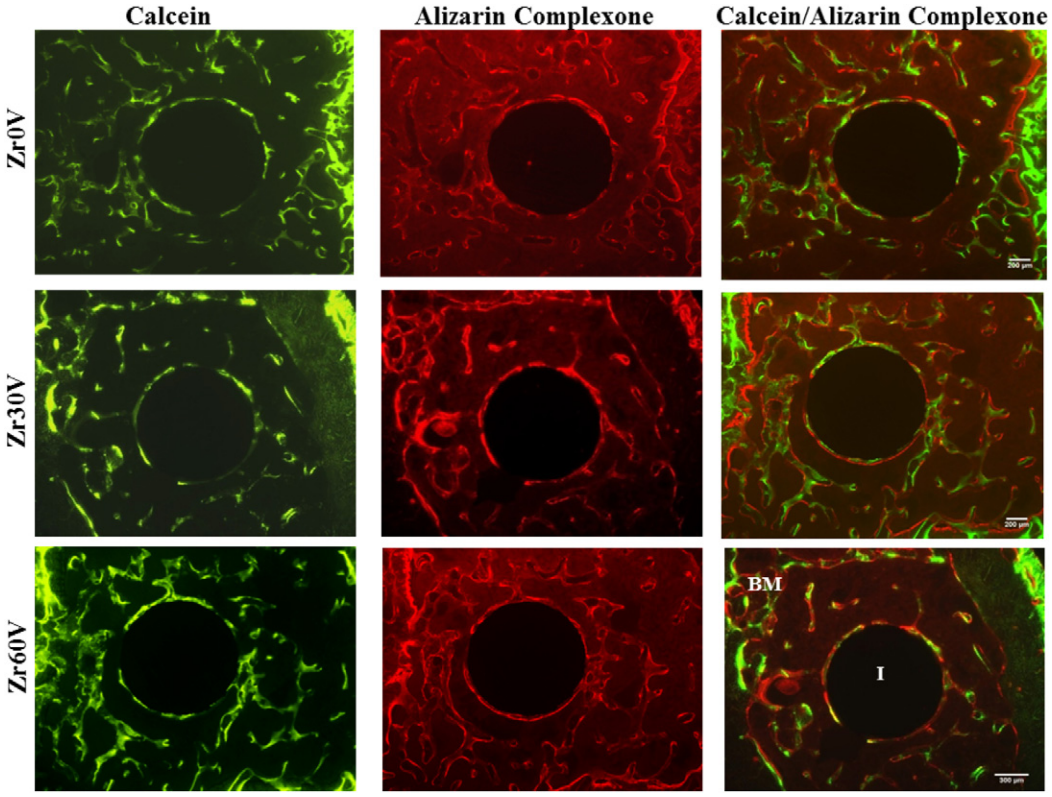

Fig. 12. Fluorescent microscopy image of rat tibia cross-sections with control and anodised implants 30 days after surgery. Green (Calcein) and red (Alizarin Complexone) lines are seen in the new bone around the implant at 30 days after implantation. In the picture: BM: bone marrow, I: implant (original magnification: 40×). (For interpretation of the references to color in this figure, the reader is referred to the web version of this article.)

become a sign of implantation success. However, other researchers found recently differences in macrophage phenotype were shown to be regulated on surface anodised with 5 V or 20 V, where surfaces generated with 5 V caused macrophages to secrete cytokines of M2 phenotype, where the rougher 20 V surfaces were associated with an M1 phenotype. In the present study, bone homeostasis is predicted to be properly maintained on anodised samples. Macrophages fusion induced by RANKL achieved mature osteoclasts with specific TRAP activity. In addition, a higher number of osteoclasts per area in anodised treatments is detected, with a well-formed actin ring that seals the resorptive area. Furthermore, a "zipper like" actin-based superstructure could be detected over anodised treatments. This feature suggests an improvement in multinucleated osteoclast fusion and an acceleration of the process. In fact, a mature osteoclasts culture with resorptive activity is characterized for an increased TRAP expression and an active lysosome machinery [17]. Our results are in concordance with these observations, showing a healthy, differentiated and active osteoclast culture over the tested samples. Moreover, osteoclasts actin filaments are aligned following the oxide treatment, showing an intimate contact between the material surface and bone cell populations. Bone resorbing cells affect tissue healing processes, regulating the osteoblast proliferation and a correct matrix deposition rate. The association between surface texture, osteoconductive matrix formation and subsequent recruitment of osteogenic cells may be an important consideration for understanding bone regeneration processes and *in vivo* implant integration.

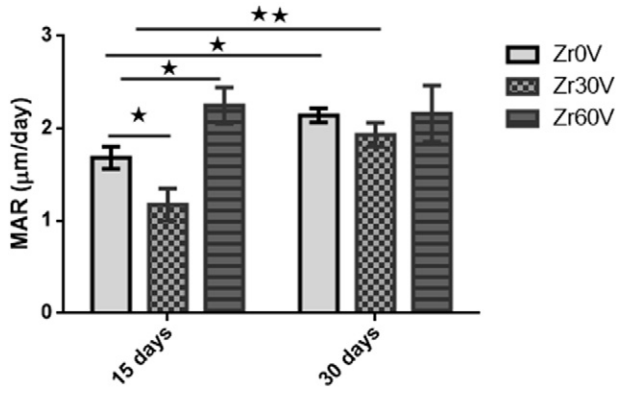

Fig. 13. Quantitative analysis of mineral apposition rate (MAR) in control and anodised implants 15 and 30 days after surgery. Values are reported as mean ± SEM. $n = 6$ femur/group (by one way ANOVA and Tukey test). $^{*}p < 0.05$.

The biological process of osseointegration of biocompatible implants can be divided roughly into four phases: first, recognition and adhesion, second, proliferation and differentiation, third synthesis and mineralization of bone matrix, and fourth, bone remodelling [60].Various kinds of coating or surface modifications on implant surfaces have been designed to regulate these four phase to promote osseointegration, either by improving the function of osteoblast lineage or by adjusting the function of osteoclast. After initial inflammatory phase which follows implant insertion [61], the subsequent bone regeneration process is strongly influenced by the implant. It is important to highlight that the forces needed to insert the implant can cause a fairly high amount of microdamage up to 500 μm away from the implant surface which, in turn, triggers a substantial but short-term increase in peri-implant bone resorption followed by formation [62]. Orthopaedic and dental implant fixation depends upon both bone-implant contact and bone formation around implant. It is well known that gaps at the interface between implant and bone increase risk of diminished implant fixation and eventual loosening [63]. To evaluate the biological response of anodisation treatment in zirconium implants in an *in vivo* model, a rat femur implantation model was used. This model has been successfully implemented by our group previously [32]. In the literature, different

time periods are used when studying implant osseointegration: animals are sacrificed after two weeks [41], four weeks [64], six weeks [65], and three month [66]. In our study we evaluated implant fixation at 15 and 30 days after implantation to assess the static and dynamic process of the bone/implant interface formation. The *in vivo* results indicate that both control and anodised zirconium implants at 30 V and 60 V have a continuous laminar bone growth on the surface of zirconium implants in rat femur with difference according to the anodisation treatment. Fifteen days after surgery, thickness of new bone formation in the periimplant bone increased substantially by surface anodisation treatment at 60 V in comparison with the values measures from control implants. Nevertheless, new bone thickness facing Zr30V implants were significant lower compared with control implant for the same time point. However, 30 days after implantation, the thickness of the new bone reached the same values in control and anodised implants. The significant increase in new bone in the trabecular was mostly due to a high MAR in this anodisation implants. By relating the increase in mineralization surface to the recruitment and MAR to the activity of osteoblast [67, 68], the results showed that anodisation treatment, principally at 60 V produce longer and faster deposition of new bone, which is reflected with newly bone thickness far from the implant surface. This transient increase in the rate of bone formation close to the implant is in agreement with previous experiments. Irish and colleagues [69] found elevated bone formation rates up to 8 weeks after the insertion of the implant into rat femur. It is important to point out that, values among different studies should be compared only qualitatively, since the studies involved different animals, implants and implantation sites. This results are in line with the results found by Guglielmonti et al. [70] suggesting that the surface modification induces a change in bone formation during the acute early phase after surgery and that after12 weeks no differences can be found between control and modified implants due to slower bone remodelling after the acute phase of new bone formation. It has been suggested that both the percentage of the implant surface covered by bone and bone thickness may improve osseointegration and anchoring of implants.

Fluorescent microscopy of the sequential fluorochrome labels revealed the dynamics of bone formation in different periods of implantation [71].The response of bone to implant is a highly dynamic process, in contrast, the main methodologies which are used to characterize it, such as histomorphometry and *in vitro* micro-computed tomography (micro-CT), are based on single time points and cannot capture the full time evolution of the structural and the remodelling changes after implant placement. Dynamic histomorphometry, for instance, allows characterizing the location and, to some extent, the time changes of bone formation (i.e. formation rate) by using multiples labels [33]. Nevertheless, the interplay between bone resorption and bone formation is of paramount importance to fully understand the net changes in bone structure occurring in the peri-implant bone, which is eventually responsible for the mechanical stability of the implant. At 15 and 30 days after implantation the two fluorescent labels calcein and alizarin complexone could be observed with similar intensity in control and both anodisation conditions. Bone apposition mineralization rate (MAR), based on fluorochrome analysis, was different between the control and anodised conditions. In the current study, 15 days after surgery the MAR of bone ingrowth and periprosthetic bone was slower on 30 V anodised zirconium implants when compared with control and interestingly 60anodisationimplants showed higher MAR values than control values fifteen days after surgery. Fluorochrome labelling profile indicates that bone extending away from the anodised implant forms at a similar rate as in control implants in the same direction. On the other hand, 30 days after surgery, in 30 V and 60 V anodisation implants, the new bone apposition MAR is lower than in control implants but no difference is possible to suggest with these results that contact osteogenesis would take place in the region facing the bone marrow at early stage of the osseointegration process. Our observations show that the bone growth rate on the surface of zirconium implant in rat femur was affected by modifying the surface, even 15 days after surgery, suggesting that the anodisation process would stimulate the osseointegration process.

The effect of surface characteristic on cells, by physicochemical interactions, generally occurs at the initial stage of cell attachment. The initial cell behaviour on the interface of cell-anodised zirconium will influence the cell differentiation, proliferation and matrix formation. In other words, the surface characteristics, topography, roughness and chemistry will adjust cell growth and at last point the success of a biomaterial.

5. Conclusions

The results provide evidence that the anodising process on Zr assesses a substrate modification that allows bone cell adhesion and proliferation, affecting cytoskeleton alignment and permitting bone cell differentiation and *in vivo* mineral apposition rate and new bone thickness at early stages after the surgery, positioning the Zr as a promising candidate as permanent cementless implant. It is important to note that after 30 days of implantation, results on modified and pristine substrates are comparable regarding the studied properties, but the processes are accelerated in the Zr60V showing a faster response for bone formation. This fact is especially important since it can shorter the recovery time for application in patients.

Acknowledgements

The support from the Consejo Nacional de Investigaciones Científicas y Técnicas (CONICET), from the Universidad Nacional de Mar del Plata (Project 15G/331) and from the Ministerio de Cliencia, Tecnologia e Innovacion Productiva (MINCyT) (Project PICT-14-1452) are acknowledge. The authors also acknowledge Mr. Sebastian Rodriguez, INTEMA, Argentina for his help in sample preparation.

In memory of Professor José Luis Lopez Lacomba, head of Tissue Engineering Group (IEB/UCM). This work was financially supported by CONSOLIDER project; CSD2009-00088). We also thank Noricum S.L. for its support in the cell studies.

References

[1] G.W. Hastings, Biomedical engineering and materials for orthopaedic implants, Journal of Physics E: Scientific Instruments 13 (6) (1980) 599.
[2] M. Navarro, A. Michiardi, O. Castaño, J.A. Planell, Biomaterials in orthopaedics, J. R. Soc. Interface 5 (27) (2008) 1137–1158, http://dx.doi.org/10.1098/rsif.2008.0151.
[3] G. Mendonca, D. Mendonca, F. Aragao, L. Cooper, Advancing dental implant surface technology—from micron- to nanotopography, Biomaterials 29 (28) (2008) 3822–3835.
[4] E. Navarro, A. Baun, R. Behra, N. Hartmann, J. Filser, A. Miao, A. Quigg, P. Santschi, L. Sigg, Environmental behavior and ecotoxicity of engineered nanoparticles to algae, plants, and fungi, Ecotoxicology 17 (5) (2008) 372–386.
[5] L. Bonsignore, J. Anderson, Z. Lee, V. Goldberg, E. Greenfield, Adherent lipopolysaccharide inhibits the osseointegration of orthopedic implants by impairing osteoblast differentiation, Bone 52 (1) (2013) 93–101.
[6] J. Davies, Understanding peri-implant endosseous healing, J. Dent. Educ. 67 (8) (2003) 932–949.
[7] J. Moreland, M. Moreno, Cementless femoral revision arthroplasty of the hip: minimum 5 years followup, Clin. Orthop. Relat. Res. 393 (2001) 194–201.
[8] R. Emerson Jr., W. Head, C. Emerson, W. Rosenfeldt, L. Higgins, A comparison of cemented and cementless titanium femoral components used for primary total hip arthroplasty: a radiographic and survivorship study, J. Arthroplasty 17 (5) (2002) 584–591.
[9] H. Yamada, Y. Yoshihara, O. Henmi, M. Morita, Y. Shiromoto, T. Kawano, A. Kanaji, K. Ando, M. Nakagawa, N. Kosaki, E. Fukaya, Cementless total hip replacement: past, present, and future, J. Orthop. Sci. 14 (2) (2009) 228–241.
[10] D. McInnis, G. Horne, P. Devane, Femoral revision with a fluted, tapered, modular stem seventy patients followed for a mean of 3.9 years, J. Arthroplasty 21 (3) (2006) 372–380.
[11] F. Matassi, C. Carulli, R. Civinini, M. Innocenti, Cemented versus cementless fixation in total knee arthroplasty, Joints 1 (3) (2013) 121–125.
[12] N. Donos, S. Hamlet, N. Lang, G. Salvi, G. Huynh-Ba, D. Bosshardt, S. Ivanovski, Gene expression profile of osseointegration of a hydrophilic compared with a hydrophobic microrough implant surface, Clin. Oral Implants Res. 22 (4) (2011) 365–372.
[13] S. Lossdorfer, Z. Schwartz, L. Wang, C. Lohmann, J. Turner, M. Wieland, D. Cochran, B. Boyan, Microrough implant surface topographies increase osteogenesis by reducing osteoclast formation and activity, J. Biomed. Mater. Res. A 70 (3) (2004) 361–369.

[14] J. Martin, D. Dean, D. Cochran, J. Simpson, B. Boyan, Z. Schwartz, Proliferation, differentiation, and protein synthesis of human osteoblast-like cells (MG63) cultured on previously used titanium surfaces, Clin. Oral Implants Res. 7 (1) (1996) 27–37.
[15] G. Schneider, H. Perinpanayagam, M. Clegg, R. Zaharias, D. Seabold, J. Keller, C. Stanford, Implant surface roughness affects osteoblast gene expression, J. Dent. Res. 82 (5) (2003) 372–376.
[16] I. Wall, N. Donos, K. Carlqvist, F. Jones, P. Brett, Modified titanium surfaces promote accelerated osteogenic differentiation of mesenchymal stromal cells in vitro, Bone 45 (1) (2009) 17–26.
[17] W. Boyle, W. Simonet, D. Lacey, Osteoclast differentiation and activation, Nature 423 (6937) (2003) 337–342.
[18] L. Wu, F. Feyerabend, A.F. Schilling, R. Willumeit-Römer, B.J.C. Luthringer, Effects of extracellular magnesium extract on the proliferation and differentiation of human osteoblasts and osteoclasts in coculture, Acta Biomater. 27 (2015) 294–304, http://dx.doi.org/10.1016/j.actbio.2015.08.042.
[19] T. Phan, J. Xu, M. Zheng, Interaction between osteoblast and osteoclast: impact in bone disease, Histol. Histopathol. 19 (4) (2004) 1325–1344.
[20] S. Marino, J.G. Logan, D. Mellis, M. Capulli, Generation and culture of osteoclasts, BoneKEy Reports 3 (2014) 570, http://dx.doi.org/10.1038/bonekey.2014.65.
[21] A.F. Mavrogenis, G.N. Nomikos, V.I. Sakellariou, G.I. Karaliotas, P. Kontovazenitis, P.J. Papagelopoulos, Wear debris pseudotumor following total knee arthroplasty: a case report, J Med Case Reports 3 (2009), http://dx.doi.org/10.1186/1752-1947-3-9304.
[22] W. Kenneth Ward, A review of the foreign-body response to subcutaneously-implanted devices: the role of macrophages and cytokines in biofouling and fibrosis, Journal of Diabetes Science and Technology (Online) 2 (5) (2008) 768–777.
[23] T. Albrektsson, C. Dahlin, T. Jemt, L. Sennerby, A. Turri, A. Wennerberg, Is marginal bone loss around oral implants the result of a provoked foreign body reaction? Clin. Implant Dent. Relat. Res. 16 (2) (2014) 155–165.
[24] R. Trindade, T. Albrektsson, P. Tengvall, A. Wennerberg, Foreign body reaction to biomaterials: on mechanisms for buildup and breakdown of osseointegration, Clin. Implant Dent. Relat. Res. 18 (1) (2016) 192–203.
[25] V. Sollazzo, F. Pezzetti, A. Scarano, A. Piattelli, C. Bignozzi, L. Massari, G. Brunelli, F. Carinci, Zirconium oxide coating improves implant osseointegration in vivo, Dent. Mater. 24 (3) (2008) 357–361.
[26] A. Yamamoto, R. Honma, M. Sumita, Cytotoxicity evaluation of 43 metal salts using murine fibroblasts and osteoblastic cells, J. Biomed. Mater. Res. 39 (2) (1998) 331–340.
[27] T. Albrektsson, C. Johansson, Osteoinduction, osteoconduction and osseointegration, Eur. Spine J. 10 (Suppl. 2) (2001) S96–101, http://dx.doi.org/10.1007/s005860100282.
[28] Y. Sul, C. Johansson, S. Petronis, A. Krozer, Y. Jeong, A. Wennerberg, T. Albrektsson, Characteristics of the surface oxides on turned and electrochemically oxidized pure titanium implants up to dielectric breakdown: the oxide thickness, micropore configurations, surface roughness, crystal structure and chemical composition, Biomaterials 23 (2) (2002) 491–501.
[29] A.G. Sanchez, W. Schreiner, G. Duffo, S. Cere, Surface characterization of anodized zirconium for biomedical applications, Appl. Surf. Sci. 257 (15) (2011) 6397–6405, http://dx.doi.org/10.1016/j.apsusc.2011.02.005.
[30] S.A. Gomez, J. Ballarre, J. Orellano, G. Duffo, S. Cere, Surface modification of zirconium by anodisation as material for permanent implants: in vitro and in vivo study, J. Mater. Sci. Mater. Med. 24 (1) (2013) 161–169.
[31] R. Hoerth, M. Katunar, S.A. Gomez, J. Orellano, S. Cere, W. Wagermaier, J. Ballarre, A comparative study of zirconium and titanium implants in rat: osseointegration and bone material quality, J. Mater. Sci. Mater. Med. 25 (2) (2014) 411–422.
[32] M.R. Katunar, A. Gomez Sanchez, J. Ballarre, M. Baca, C. Vottola, J.C. Orellano, H. Schell, G. Duffo, S. Cere, Can anodised zirconium implants stimulate bone formation? Preliminary study in rat model, Progress in Biomaterials 3 (1) (2014) 1–10, http://dx.doi.org/10.1007/s40204-014-0024-9.
[33] H. Kajiwara, T. Yamaza, M. Yoshinari, T. Goto, S. Iyama, I. Atsuta, M. Kido, T. Tanaka, The bisphosphonate pamidronate on the surface of titanium stimulates bone formation around tibial implants in rats, Biomaterials 26 (6) (2005) 581–587.
[34] J.J.P. Jaatinen, R.K. Korhonen, A. Pelttari, H.J. Helminen, H. Korhonen, R. Lappalainen, H. Kröger, Early bone growth on the surface of titanium implants in rat femur is enhanced by an amorphous diamond coating, Acta Orthop. 82 (4) (2011) 499–503, http://dx.doi.org/10.3109/17453674.2011.579522.
[35] Kruyt M. van GS, R. Geuze, Alblas J. de BJ, W. Dhert, Use of fluorochrome labels in in vivo bone tissue engineering research, Tissue Eng. Part B Rev. 16 (2) (2010) 209–217.
[36] Jiang X-q, S.-y. Wang, J. Zhao, Zhang X-l, Zhang Z-y, Sequential fluorescent labeling observation of maxillary sinus augmentation by a tissue-engineered bone complex in canine model, Int. J. Oral Sci. 1 (1) (2009) 39–46, http://dx.doi.org/10.4248/ijos.08022.
[37] A. Parfitt, M. Drezner, F. Glorieux, J. Kanis, H. Malluche, P. Meunier, S. Ott, R. Recker, Bone histomorphometry: standardization of nomenclature, symbols, and units. Report of the ASBMR Histomorphometry Nomenclature Committee, J. Bone Miner. Res. 2 (6) (1987) 595–610.
[38] L. Aloia Games, A. Gomez Sanchez, E. Jimenez-Pique, W.H. Schreiner, S.M. Ceré, J. Ballarre, Chemical and mechanical properties of anodized cp-titanium in NH_4 H 2PO 4/NH 4F media for biomedical applications, Surf. Coat. Technol. 206 (23) (2012) 4791–4798, http://dx.doi.org/10.1016/j.surfcoat.2012.03.092.
[39] A. Gomez-Sanchez, M. Katunar, W. Schreiner, G. Duffo, S. Cere, D. Schiffrin, Structure and dielectric properties of electrochemically grown ZrO_2 films, Acta Chim. Slov. 61 (2) (2014) 316–327.
[40] Z. Chen, T. Klein, R.Z. Murray, R. Crawford, J. Chang, C. Wu, Y. Xiao, Osteoimmunomodulation for the development of advanced bone biomaterials, Mater. Today 19 (6) (2016) 304–321, http://dx.doi.org/10.1016/j.mattod.2015.11.004.
[41] P. Tengvall, B. Skoglund, A. Askendal, P. Aspenberg, Surface immobilized bisphosphonate improves stainless-steel screw fixation in rats, Biomaterials 25 (11) (2004) 2133–2138.
[42] F. Boccafoschi, C. Mosca, M. Cannas, Cardiovascular biomaterials: when the inflammatory response helps to efficiently restore tissue functionality? J. Tissue Eng. Regen. Med. 8 (4) (2014) 253–267.
[43] J. Morais, F. Papadimitrakopoulos, D. Burgess, Biomaterials/tissue interactions: possible solutions to overcome foreign body response, AAPS J. 12 (2) (2010) 188–196.
[44] M. Rahmany, D.M. Van, Biomimetic approaches to modulate cellular adhesion in biomaterials: a review, Acta Biomater. 9 (3) (2013) 5431–5437.
[45] T. Betancourt, L. Brannon-Peppas, Micro- and nanofabrication methods in nanotechnological medical and pharmaceutical devices, Int. J. Nanomedicine 1 (4) (2006) 483–495.
[46] A. Refai, M. Textor, D. Brunette, J. Waterfield, Effect of titanium surface topography on macrophage activation and secretion of proinflammatory cytokines and chemokines, J. Biomed. Mater. Res. A 70 (2) (2004) 194–205.
[47] W. Soskolne, S. Cohen, L. Sennerby, A. Wennerberg, L. Shapira, The effect of titanium surface roughness on the adhesion of monocytes and their secretion of TNF-alpha and PGE2, Clin. Oral Implants Res. 13 (1) (2002) 86–93.
[48] J. Gamboa, S. Mohandes, P. Tran, M. Slepian, J. Yoon, Linear fibroblast alignment on sinusoidal wave micropatterns, Colloids Surf. B Biointerfaces 104 (2013) 318–325.
[49] M. Hulander, A. Lundgren, L. Faxalv, T. Lindahl, A. Palmquist, M. Berglin, H. Elwing, Gradients in surface nanotopography used to study platelet adhesion and activation, Colloids Surf. B Biointerfaces 110 (2013) 261–269.
[50] V. Vogel, M. Sheetz, Local force and geometry sensing regulate cell functions, Nat. Rev. Mol. Cell Biol. 7 (4) (2006) 265–275.
[51] C. Gilchrist, D. Ruch, D. Little, F. Guilak, Micro-scale and meso-scale architectural cues cooperate and compete to direct aligned tissue formation, Biomaterials 35 (38) (2014) 10015–10024.
[52] Q. Ma, L. Zhao, R. Liu, B. Jin, W. Song, Y. Wang, Y. Zhang, L. Chen, Y. Zhang, Improved implant osseointegration of a nanostructured titanium surface via mediation of macrophage polarization, Biomaterials 35 (37) (2014) 9853–9867.
[53] K. Tan, L. Qian, R. Rosado, P. Flood, L. Cooper, The role of titanium surface topography on J774A.1 macrophage inflammatory cytokines and nitric oxide production, Biomaterials 27 (30) (2006) 5170–5177.
[54] J. Lopacinska, C. Gradinaru, R. Wierzbicki, C. Kobler, M. Schmidt, M. Madsen, M. Skolimowski, M. Dufva, H. Flyvbjerg, K. Molhave, Cell motility, morphology, viability and proliferation in response to nanotopography on silicon black, Nanoscale 4 (12) (2012) 3739–3745.
[55] R. Gittens, T. McLachlan, R. Olivares-Navarrete, Y. Cai, S. Berner, R. Tannenbaum, Z. Schwartz, K. Sandhage, B. Boyan, The effects of combined micron-/submicron-scale surface roughness and nanoscale features on cell proliferation and differentiation, Biomaterials 32 (13) (2011) 3395–3403.
[56] S. Chen, J. Jones, Y. Xu, H. Low, J. Anderson, K. Leong, Characterization of topographical effects on macrophage behavior in a foreign body response model, Biomaterials 31 (13) (2010) 3479–3491.
[57] M. Ahmad, D. Gawronski, J. Blum, J. Goldberg, G. Gronowicz, Differential response of human osteoblast-like cells to commercially pure (cp) titanium grades 1 and 4, J. Biomed. Mater. Res. 46 (1) (1999) 121–131.
[58] A. Arranz, C. Doxaki, E. Vergadi, Y. Martinez dlT, K. Vaporidi, E. Lagoudaki, E. Ieronymaki, A. Androulidaki, M. Venihaki, A. Margioris, E. Stathopoulos, P. Tsichlis, C. Tsatsanis, Akt1 and Akt2 protein kinases differentially contribute to macrophage polarization, Proc. Natl. Acad. Sci. U. S. A. 109 (24) (2012) 9517–9522.
[59] S. Gordon, F. Martinez, Alternative activation of macrophages: mechanism and functions, Immunity 32 (5) (2010) 593–604.
[60] do A.E.A. de OJ, R.M. Alves, M. Mathor, C.A. Alves, Analysis of the effects of irradiation in osseointegrated dental implants, Clin. Oral Implants Res. 23 (4) (2012) 511–514.
[61] F. Marco, F. Milena, G. Gianluca, O. Vittoria, Peri-implant osteogenesis in health and osteoporosis, Micron 36 (7–8) (2005) 630–644.
[62] L. Wang, T. Ye, L. Deng, J. Shao, J. Qi, Q. Zhou, L. Wei, S. Qiu, Repair of microdamage in osteonal cortical bone adjacent to bone screw, PLoS One 9 (2) (2014), e89343. http://dx.doi.org/10.1371/journal.pone.0089343.
[63] Y. Gao, E. Luo, J. Hu, J. Xue, S. Zhu, J. Li, Effect of combined local treatment with zoledronic acid and basic fibroblast growth factor on implant fixation in ovariectomized rats, Bone 44 (2) (2009) 225–232, http://dx.doi.org/10.1016/j.bone.2008.10.054.
[64] R.A. De, A. Virdi, S. Kuroda, S. Shott, R. Leven, N. Hallab, D. Sumner, Local application of rhTGF-beta2 enhances peri-implant bone volume and bone-implant contact in a rat model, Bone 37 (1) (2005) 55–62.
[65] Y. Gabet, D. Kohavi, T. Kohler, M. Baras, R. Muller, I. Bab, Trabecular bone gradient in rat long bone metaphyses: mathematical modeling and application to morphometric measurements and correction of implant positioning, J. Bone Miner. Res. 23 (1) (2008) 48–57.
[66] Y. Gao, S. Zou, X. Liu, C. Bao, J. Hu, The effect of surface immobilized bisphosphonates on the fixation of hydroxyapatite-coated titanium implants in ovariectomized rats, Biomaterials 30 (9) (2009) 1790–1796.
[67] A. Birkhold, H. Razi, G. Duda, R. Weinkamer, S. Checa, B. Willie, Mineralizing surface is the main target of mechanical stimulation independent of age: 3D dynamic in vivo morphometry, Bone 66 (2014) 15–25.
[68] F. Lambers, K. Koch, G. Kuhn, D. Ruffoni, C. Weigt, F. Schulte, R. Muller, Trabecular bone adapts to long-term cyclic loading by increasing stiffness and normalization of dynamic morphometric rates, Bone 55 (2) (2013) 325–334.
[69] J. Irish, A. Virdi, K. Sena, M. McNulty, D. Sumner, Implant placement increases bone remodeling transiently in a rat model, J. Orthop. Res. 31 (5) (2013) 800–806.
[70] M. Guglielmotti, S. Renou, R. Cabrini, A histomorphometric study of tissue interface by laminar implant test in rats, Int. J. Oral Maxillofac. Implants 14 (4) (1999) 565–570.
[71] Y. Huang, X. Jin, X. Zhang, H. Sun, J. Tu, T. Tang, J. Chang, K. Dai, In vitro and in vivo evaluation of akermanite bioceramics for bone regeneration, Biomaterials 30 (28) (2009) 5041–5048.